ORIGINAL PAPER

Effective nanocomposite flexible electrochemical storage with Li⁺/PVdF-HFP/PEO/n-ZrO$_2$ complex

P. Ajay Kumar[1,2] · A. Mallikarjun[3,4] · M. Maheshwar Reddy[1,5] · M. Jaipal Reddy[6] · J. Siva Kumar[1]

Abstract

In order to enhance storage capacity and prevent electrical short circuits in electrochemical storage devices, it is essential and challenging to design and build Lithium ion batteries with flexible solid polymer electrolyte possessing strong ionic conductivity. This study details the use of solution-cast technique to create nano composite doped lithium solid polymer electrolytes (n-LSPEs), from polymer complex of poly (vinylidene fluoride-co-hexafluoropropylene) (PVdF-HFP), polyethylene oxide (PEO), and Lithium trifluoromethanesulfonate (LiCF$_3$SO$_3$), with nano ZrO$_2$ (n-ZrO$_2$). Electrochemical impedance spectroscopy (EIS) was utilised to describe the ionic conductivity values in presence of alternating fields. The ionic conductivity of n-LSPEs are enhanced nearly four times (1.54×10^{-1} mS/cm to 5.996×10^{-1} mS/cm) due to addition of n-ZrO$_2$. By incorporating chronoamperometry (CA) and cyclic voltammetry (CV), we were able to analyse the transference number, ionic strength, and the accumulation of charge carriers in optimized n-LSPE membrane. Scanning electron microscope (SEM) images of n-LSPE membranes reveal a structure that is consistent with interconnecting pores between the polymer complex and the nano filler. The stable monoclinic phase of n-ZrO$_2$ interaction with polymer segmental motion was confirmed by X-ray diffraction (XRD). By examining Fourier transform infrared spectroscopy (FTIR), we performed a quick analysis of the complexation of functional group investigations, bond length and force constant calculations, interaction of functional groups of n-LSPE films. Our FESD's discharge characteristics were investigated at 4.8 mA average discharge current for 25 hours, as indicated by a 0.04C rating.

Keywords n-LSPEs · FESD · EIS · CA · CV · SEM · XRD · FTIR · etc.

✉ P. Ajay Kumar
 ajayphy1729@gmail.com

1 Department of Physics, Osmania University, Hyderabad, Telangana, India

2 Department of Science and Humanities and Department of Technical Education, Government Polytechnic, Gadwal, Telangana, India

3 Department of Science and Humanities, Vignan's Institute of Management and Technology for Women, Hyderabad, Telangana, India

4 Department of Science and Humanities, JNTUH, Hyderabad, Telangana, India

5 Department of Science and Humanities, Sreenidhi Institute of Science and Technology, Hyderabad, Telangana, India

6 Department of Physics, Palamuru University, Mahabubnagar, Telangana, India

Introduction

In the realm of modern smart electronic technology (SET) devices, flexible electrochemical storage devices (FESDs) are prominent key carriers because of their low cost, lighter weight, efficient life cycle durability, and high power and energy densities. FESDs are the foundational technologies for wearables, sensors, electric cars, flexible (foldable and stretchable) electronics, and other portable integrated consumer electronics. For electrochemical energy storage applications [1], nano composite doped lithium solid polymer electrolytes (n-LSPEs) are overwhelmingly amazing in maintaining the adaptability, mechanical stability, and high conductivity qualities of FESDs [2–4]. Blended polymer complexes are recognised as excellent host materials for n-LSPEs because they offer a wide range of mechanisms for bringing about structural modifications, salt dissociation, and charge transport enhancements in n-LSPEs. Due to their superior electrochemical properties, blended polymer

complexes have greatly benefited rechargeable batteries, fuel cells, sensors, super capacitors, dye-sensitized solar cells (DSSC), electric vehicles and FESDs, RFID tags, SETDs, and other devices [5–8]. Since $LiCF_3SO_3$ has the highest dissociation constant of all lithium salts and significantly alters thermomechanical, miscibility, dielectric, electrical, crystallinity, and polymeric chain segmental dynamics, it piques the interest of researchers looking into lithium based polymer blend electrolytes [9, 10]. In particular, nano composites doped polymer complexes accentuating researchers in the arena of diversified manufacturing zones occupied by electrochemical storage devices, rechargeable batteries, solar cells, sensors, electric vehicles, smart electronic technology devices were owing to strengthened electrical, optical, and mechanical stuff [11–16].

Zirconia (ZrO_2) nanoparticles are effective among metal oxides into sandwiching with organic matrices creates extreme technological pertinence, enhanced strength, toughness modification, excellent resisting capability of chemical, microbial and corrosion. ZrO_2 is a p-type semiconductor with large band gap manifest plentiful oxygen vacancies. It is a good catalyst owing to enhanced redox activity, strengthened ion exchange proportions. ZrO_2 insulating asset and its extensive thermostable behaviour has applications in nano electronic devices, fuel cells, gas sensing of oxygen and nitrogen oxide. An excellent optical and electrical domains of Zirconia nanoparticles makes highly attentive in broad range of applications corresponds to electro-optic, dielectric and piezoelectric devices [17–23].

This research involves the preparation of *n*-LSPEs using ‖ PVdF-HFP: PEO: $LiCF_3SO_3$: *n*-ZrO_2 ‖ complexes and the subsequent examination of these materials at the structural, morphological, and electrochemical levels. We have developed FESD based on optimized *n*-LSPE membrane and investigated discharge characteristics.

Experimental section

Materials used

PVdF-HFP was used as the main polymer in this study, with CAC:14,283–07-9, PEO as the co-polymer with CAS:25,322–68-3, Lithium trifluoromethanesulfonate ($LiCF_3SO_3$) with CAS:33,454–82-9, *n*-ZrO_2 powder, and V_2O_5 powder, all procured from Sigma Aldrich. For this purpose, we sourced our tetrahydrofuran (Emparta AR grade), Toluene (Emparta AR grade) solvents and acetone (Emparta AR grade) cleaning agent from Merck Millipore, Germany. The electrodes consisted of lithium carbonate (Li_2CO_3) from Sigma Aldrich and cupric sulphate ($CuSO_4.5H_2O$) from SD Fine Chemicals. We analysed our cole–cole plots with ZSimpWin, a free programme.

Preparation of *n*-LSPEs (PVdF-HFP: PEO: $LiCF_3SO_3$: *n*-ZrO_2)

To fabricate our nano composite doped lithium solid polymer blend electrolytes (*n*-LSPEs), we have used the solution cast method. THF solvent was used to combine and disperse the polymer complex ‖ PVdF-HFP: PEO: $LiCF_3SO_3$ ‖ contained a targeted weight ratio of *n*-ZrO_2. The ‖PVdF-HFP: PEO: $LiCF_3SO_3$‖ complex was doped with *n*-ZrO_2 at concentrations of 5 mg, 10 mg, 15 mg, 20 mg, and 25 mg to determine the influence of the *n*-ZrO_2 at these low doses on the PLZ0 ionic conductivity. The solutions were stirred with a REMI 2MLH magnetic stirrer at 60 °C for 2 h and then at room temperature for 24 h, until homogeneity was achieved. The prepared homogenous solutions were then cast in petri dishes by achieving solvent evaporation and drying at a slow rate in a vacuum oven at 60 °C for 48 h. By adopting this technique, you will be able to create polymer films that have good mechanical stability and are capable of standing on their own [24]. The *n*-LSPEs that were made were labelled with their respective compositions from PLZ0 to PLZ5. We have chosen in order to protect the films from humidity interaction and keep them in good enough condition for characterization studies, they were stored in a desiccator until they were ready to be used Table 1 contains a comprehensive breakdown of manufactured film specifications.

Results and discussions

Electrochemical analysis

Electrochemical analysis is a starting point for investigating a comprehensive approach to interrogating electrolytes for electrochemical storage devices and their related applications, such as rechargeable batteries, super capacitors,

Table 1 ‖ PVdF-HFP: PEO: $LiCF_3SO_3$: *n*-ZrO_2 ‖ complexes with their weight ratios

Sample	PVdF-HFP (g)	PEO (g)	$LiCF_3SO_3$ (g)	*n*-ZrO_2 (g)
PLZ0	1	0.1	0.4	0
PLZ1	1	0.1	0.4	0.005
PLZ2	1	0.1	0.4	0.010
PLZ3	1	0.1	0.4	0.015
PLZ4	1	0.1	0.4	0.020
PLZ5	1	0.1	0.4	0.025

sensors in electric vehicles, and smart electronic technology devices. The current study's electrochemical analysis included impedance, dielectric, amperometry, and voltammetry measurements.

Impedance spectroscopy

The ionic conductivity calculations have been carried out using complex impedance analysis which depicts ion dynamics in polymer electrolytes based on bulk resistance (R_b). The traditional impedance spectroscopy method involves the study of variation between real impedance Z′ (as a function of frequency) and imaginary impedance Z″ (as a function of frequency) is also known as complex impedance plots or Nyquist plots [25, 26]. The complex impedance plots of PLZ films were fitted in circles using origin software. Bulk resistance (R_b) values of PLZ films were attained from intercepts of real impedance axis (Z′). Ionic conductivity values of fabricated PLZ films have been calculated using following relation [25].

$$\sigma(\text{S/cm}) = \frac{t}{A \times R_b} \tag{1}$$

where, t- thickness, A- Area of cross section, and R_b- Bulk resistance of PLZ films. The Nyquist plots of n-ZrO_2 doped ‖ PVdF-HFP: PEO: $LiCF_3SO_3$ ‖ complexes (n-LSPEs) at room temperature were shown in Fig. 1a. The equivalent circuit of optimized sample of Nyquist plot was analysed and embedded in Fig. 1a, using ZSimpWin free software. Nyquist plots of PLZ films at room temperature are shown in Fig. 1a. Sample Nyquist plot from PLZ4 results the equivalent circuit as incorporated
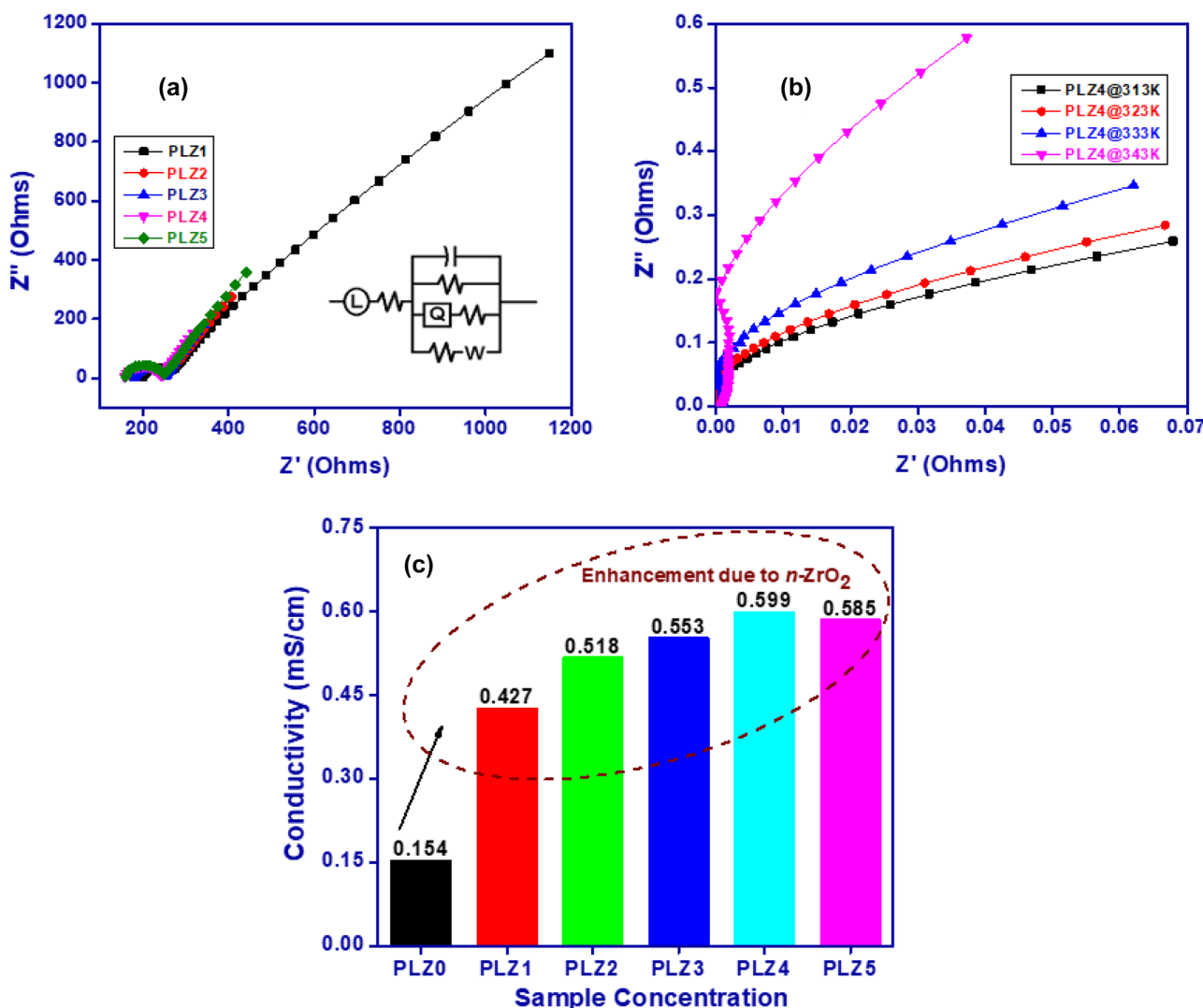

Fig. 1 **a** Nyquist plots of PLZ films at room temperature **b** PLZ4 Nyquist plots with temperature variation **c** Ionic conductivity variation of PLZ films with various concentration n-ZrO_2

(Fig. 1a). Nyquist plots are characterised by a semicircle at the beginning, followed by a peak line at the end, when viewed in the frequency domain. High-frequency effects are attributed to ion movement and inflexible polymer networks due to the parallel combination of bulk resistance and bulk capacitance, whereas low-frequency effects are attributed to constant phase elements (Q) and Warburg impedance (W) effects. The spike length after semicircle exhibits the impact of polarisation at the electrode/electrolyte interface. As the n-ZrO$_2$ concentration grows, smaller and smaller semicircles are created in Nyquist plots, which confirms decreasing in bulk resistance. The analogous circuit demonstrates the existence of a constant phase element and a Warburg dispersive impedance, the latter of which is due to the interconnectedness of the porous polarisation network. The most efficient interconnected porous network can be found in the polymer electrolyte PLZ4, which enables the creation of a truncated constant phase element and a Warburg impedance. In general, when polarisation resistance developed due to capacitive elements at high frequency, the porous nature of the polymer electrolyte film surface interacted and communicated with the electrodes. The presence of inductive element in equivalent circuit (Fig. 1a) signifies interaction of n-ZrO$_2$ with salt increases inductive effect leads to raise in ion dissociation and hence conductivity increases [27].

The Nyquist plots of PLZ4 at different temperatures are shown in Fig. 1(b). When heated to high temperatures, the bulk resistance (R$_b$) values of the PLZ4 sample decrease, which is a good indicator of increased conductivity. Figure 1(c) shows that the ionic conductivity of the polymer complex rises with increasing n-ZrO$_2$ content at room temperature [28, 29].

In conclusion, the results of this study show that our n-LSPEs show improved ion transport behaviour in high n-ZrO$_2$ conditions evidences electrochemical storage applications. The optimum PLZ4 had an ionic conductivity of 5.996×10^{-1} mS/cm. Table 2. displays the results of a comparison between the estimated ionic conductivity value of the optimised sample PLZ4 and the ionic conductivity values reported for LiCF$_3$SO$_3$ based polymer electrolytes.

Dielectric studies

Dielectric studies were attentive for polymer electrolytes in energy storage applications.

The frequency dependent complex dielectric function (ε^*) denoted using following relation,

$$\varepsilon^* = \varepsilon'(\omega) - i\varepsilon''(\omega) = \frac{1}{i\omega C_0 Z^*} \tag{2}$$

where ε'-real part of complex permittivity, ε''-imaginary part of complex permittivity, ω—angular frequency, C$_0$—Capacitance of material in vacuum and Z*- complex impedance respectively. Figure 2. depicts the variations in and with the frequency of PLZ films. The homologous behaviour of and in Fig. 2a, b clearly indicates that PLZ films have higher dielectric constants at lower frequencies due to electrodes polarization effects associated with ion accumulation demonstrate complete salt dissociation, and decreases towards higher frequencies are caused by space charge polarisation, polar groups, and ion orientation. At low frequencies, ion hopping and net polarisation caused by ions piling up at field-directed sites contribute to higher dielectric permittivity, whereas at high frequencies, gradual decreases in ion hopping and net polarisation caused by charge pileup due to field reversal contribute to lower dielectric permittivity.

Cole–Cole plot of dielectric constants was analysed and displayed in Fig. 2c. PLZ films are characterised by a straight line in the low frequency region and an incomplete arc in the high frequency side. Electrode polarisation at the electrode-sample interface is credited with the line, while the arc is attributed to the bulk relaxation process. The increased electrode polarisation with increased domination of n-ZrO$_2$ in the films was confirmed by the observation of a straight line dependence. Additionally, the capacitive elements present in the equivalent circuit embedded Fig. 2c signifies majorly the electrodes' polarisation, and also contributes polarisation caused by porous network of n-LSPE interface. This demonstrates that our n-LSPEs have the potential to be used as capacitors [36]. Schematic of electrode polarization and dielectric dispersions were displayed in Fig. 2d.

Table 2 Comparative analysis of our work with literature

| Polymer electrolyte composition	σ (room temperature)	Reference
PMMA- LiCF$_3$SO$_3$-SiO$_2$	7.30×10^{-2} mS/cm	Ramesh et al., (2010) [30]
PVdFHFP-LiCF$_3$SO$_3$	1.11×10^{-2} mS/cm	Alias et al. (2012) [31]
PEO-PMMA-LiCF$_3$SO$_3$-10 Wt% of PEG	2.66×10^{-2} mS/cm	Sengwa et al. (2014) [32]
PVA-PAN-LiCF$_3$SO$_3$	4×10^{-2} mS/cm	Genova et al. (2017) [33]
TSP- LiCF$_3$SO$_3$	8.37×10^{-1} mS/cm	Sampath et al. (2020) [34]
P(MMA-co-VBIm-TFSI)-PVdFHFP -LiCF$_3$SO$_3$	1.14×10^{-1} mS/cm	Zhefei et al. (2022) [35]
PVdFHFP-PEO-LiCF$_3$SO$_3$	**1.541×10^{-1} mS/cm**	**Our work**
PVdF-HFP- PEO- LiCF$_3$SO$_3$-ZrO$_2$	**5.996×10^{-1} mS/cm**	**Our work**

*mS/cm means milliSiemens per centimeter
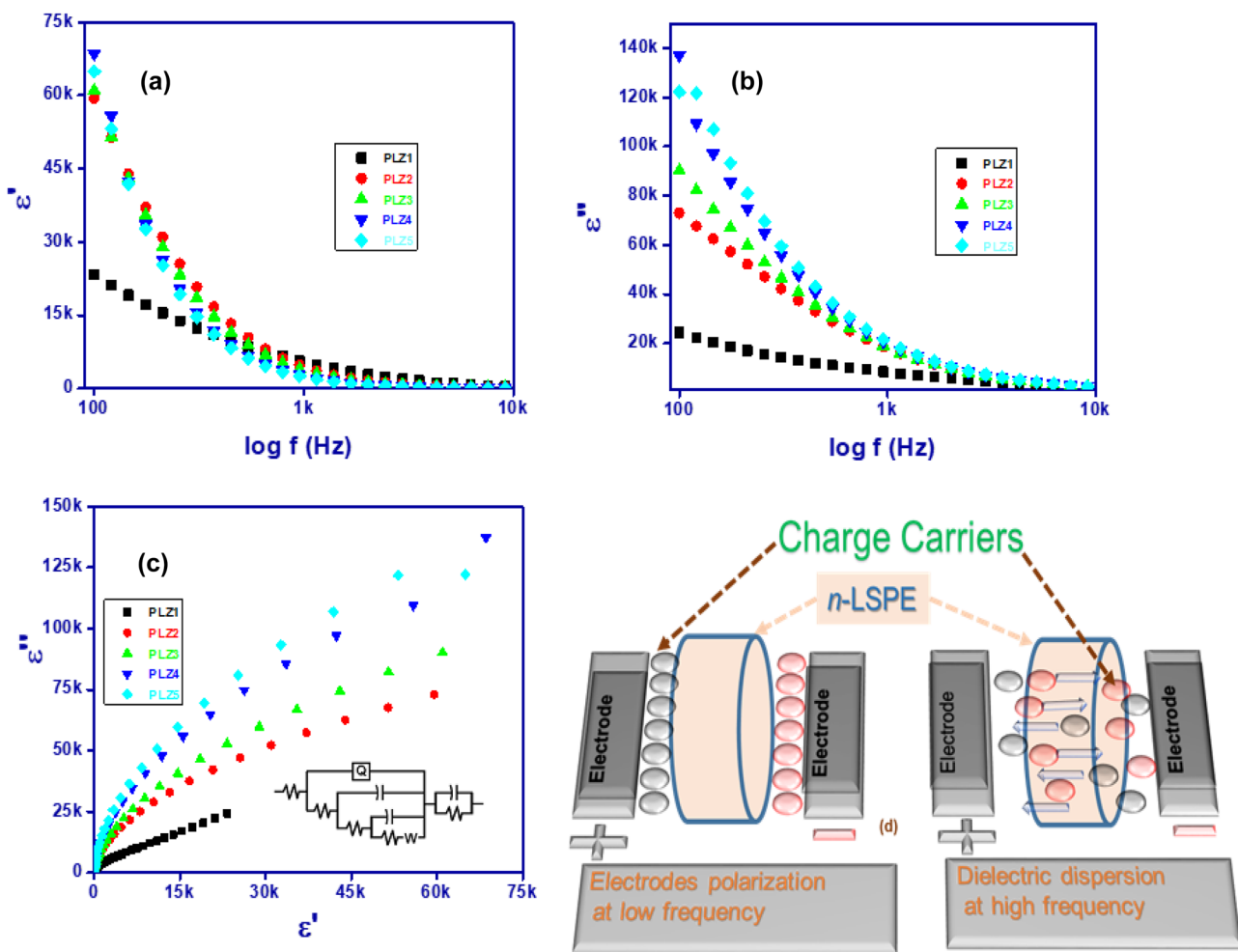
Fig. 2 **a** The real part of complex permittivity variation with frequency for PLZ films **b** The imaginary part of complex permittivity variation with frequency for PLZ films. **c** Dielectric based Cole–Cole plots of PLZ films at room temperature **d** Schematic interpretation of dielectric behavior with frequency

The measurement of dielectric loss was used as a starting point to investigate the effects of electrode polarisation and charge transfer on energy dissipation. The measurement investigates the variation of tangent loss (tan $\delta = \varepsilon'/\varepsilon''$) with frequency, as shown in Fig. 3. The PLZ samples have two sets of dielectric relaxation peaks to be observed. Tangent loss initially increases with frequency to reach its first peak at lower frequencies, then decreases and continues to reach its second relaxation maxima at higher frequencies. The first peak could be a clear indication of side group dipoles, while the second peak must be due to the movement of main chain dipole segments. Electrode polarisation effects cause the corresponding peaks at specific frequencies [36–38].

Electric modulus study

Complex electric modulus studies have huge interest reveals electrical relaxation behaviour in both electronically conducting and ionic conducting materials. The real part of

impedance (Z′) and modulus (M′) was shown in Fig. 4a. The higher values of M′ at higher frequencies confirms electrode polarization effects were negligible. The decreasing behaviour of real part impedance (Z′) with increasing in frequency indicates reduction of space charge polarization effects [39].

The real part of impedance (Z″) and modulus (M″) was depicted in Fig. 4b. The obtained peak values of M″ & Z″ values with respect to frequency results long range or short range relaxation processes. The formation of M″ peaks at higher frequency deviates from low frequency peaks of Z″ due to the localized movement of charge carriers clearly amends decamp from ideal Debye behaviour [40].

Chronoamperometry studies

Ionic transport behaviour in polymer electrolytes can be better understood through chronoamperometry research. We have used chronoamperometry to probe the ionic strength of
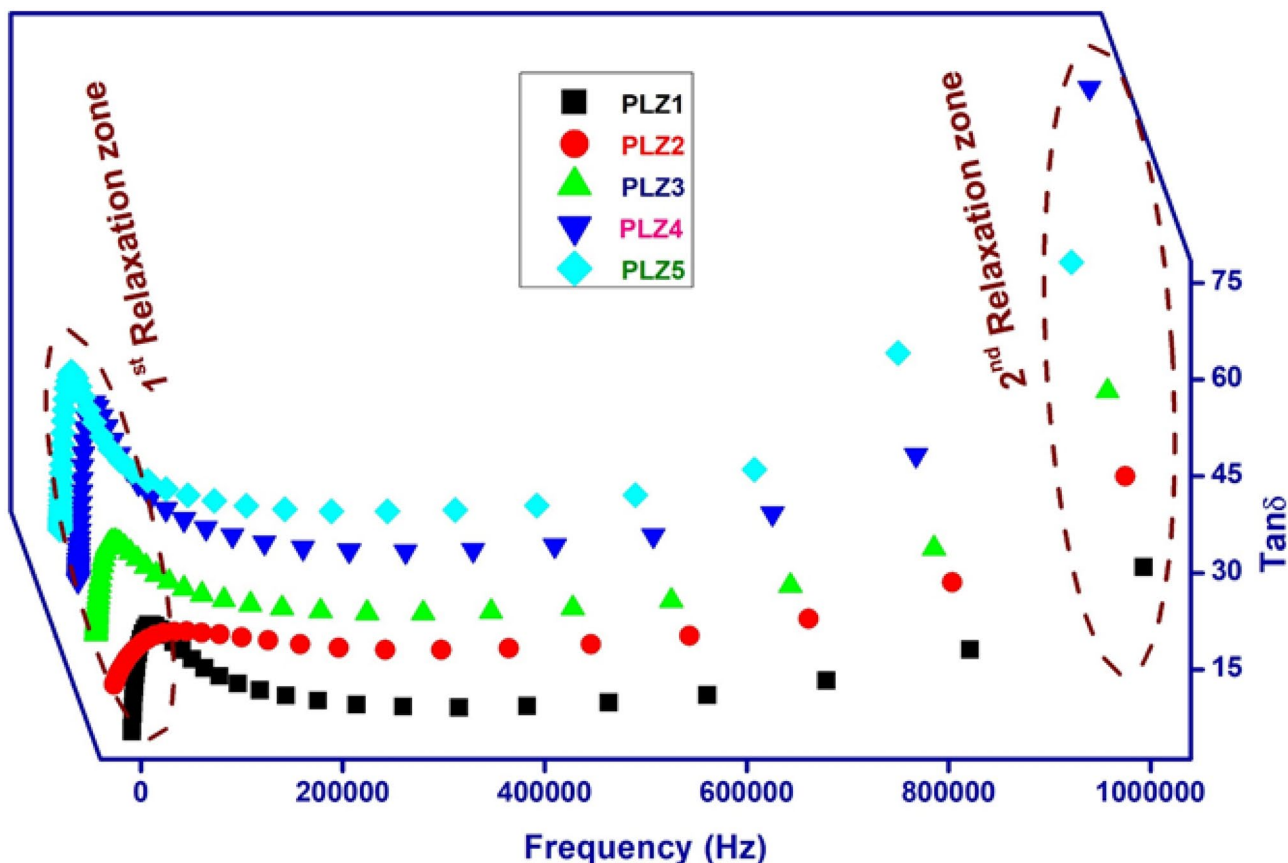
Fig. 3 Tangent loss of PLZ films at room temperature

the optimised PLZ4 sample. A double-potential step chrono-amperogram of the PLZ4 membrane shown in Fig. 5a. was used to determine the profiles of the cathode and anode currents due to *n*-LSPE membrane. It's possible that forward cycles signify the reduction mechanism while backward cycles signify the sta-bility of the oxidation process of *n*-LSPE membrane observed near the electrodes. The reduction process adds a charge during the forward stage, whereas the oxidation step removes a charge
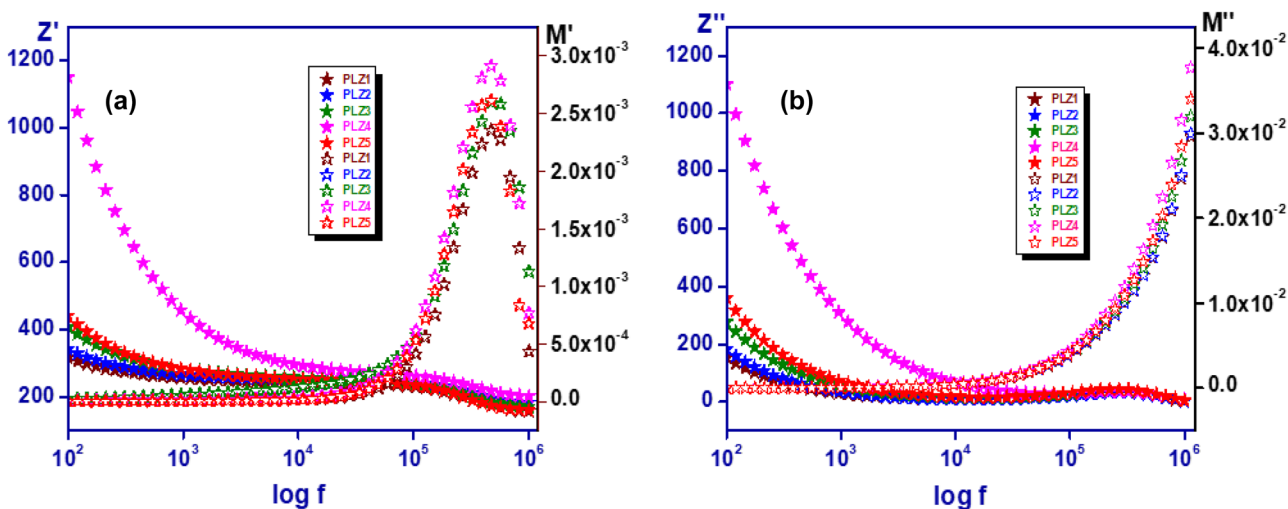
Fig. 4 a The variation of Z′ and M′ with frequency for PLZ films **b** The variation of Z″ and M″ with frequency for PLZ films
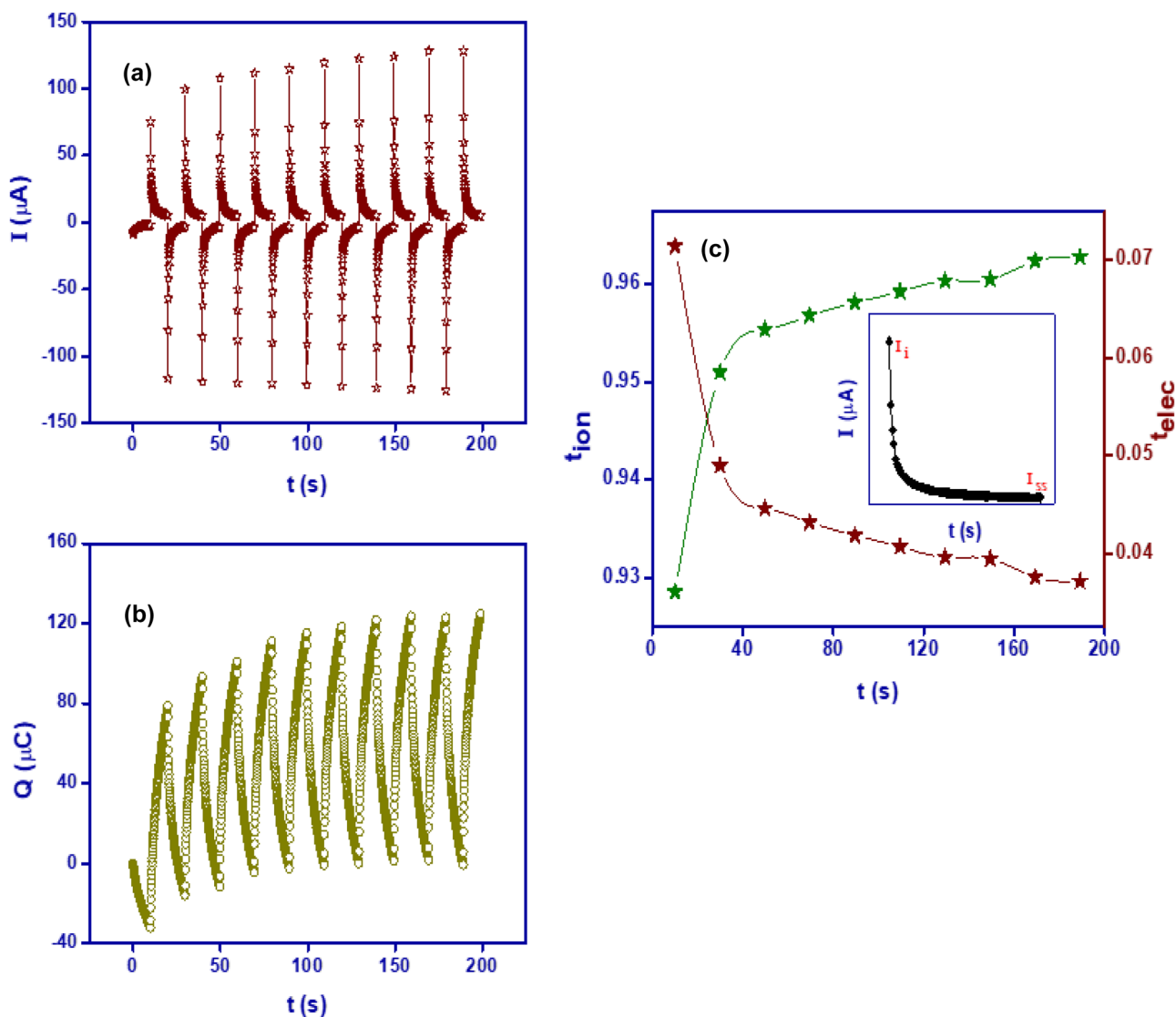
Fig. 5 **a** Chronoamperogram of PLZ4 **b** Cumulated charge transfer profile of PLZ4 **c** Transference number analysis of PLZ4

during the backward stage. To describe the variation in cathode current with time, the well-known Cottrell equation is a good approximation, $I \propto t^{-1/2}$ [41].

A rise in PLZ4's ionic activity over time may be traced back to an increase in the concentration of charge carriers, as shown in Fig. 5b, which is a result of reduction and oxidation processes involving accumulated charge (Q). Integration of the area under each curve of current versus time for each cycle was used to estimate the total charge. The increasing charge carriers from the first to the last cycle provides substantial evidence for the enhanced ionic activity of PLZ4. Further, we have estimated ion transference number (t_{ion}) and electron transference number (t_{elec}) using following relations.

$$t_{ion} = (I_i - I_{ss})/I_i \tag{3}$$

$$t_{elec} = 1 - t_{ion} \tag{4}$$

I_i = Initial current, I_{ss} = Steady state current. Initially, I_i is the current, and I_{ss} is the current in a steady state. Figure 5c depicts an increase in estimated t_{ion} values as well as a closer approach to unity. Both the t_{ion} and t_{elec} components of PLZ4 can reach their maximum values of 0.963 and 0.037, respectively. If the t_{ion} value is close to one, it shows that the electrolyte has a high ionic strength and protects the electrodes reliably over time, which is essential in the energy storage regime [42].

Cyclic voltammetry studies

The optimal conductivity sample PLZ4 was recorded in cyclic voltammograms (CV-plots) at 10 mV/s, 20 mV/s, 30 mV/s, 40 mV/s, and 50 mV/s was represented in Fig. 6.
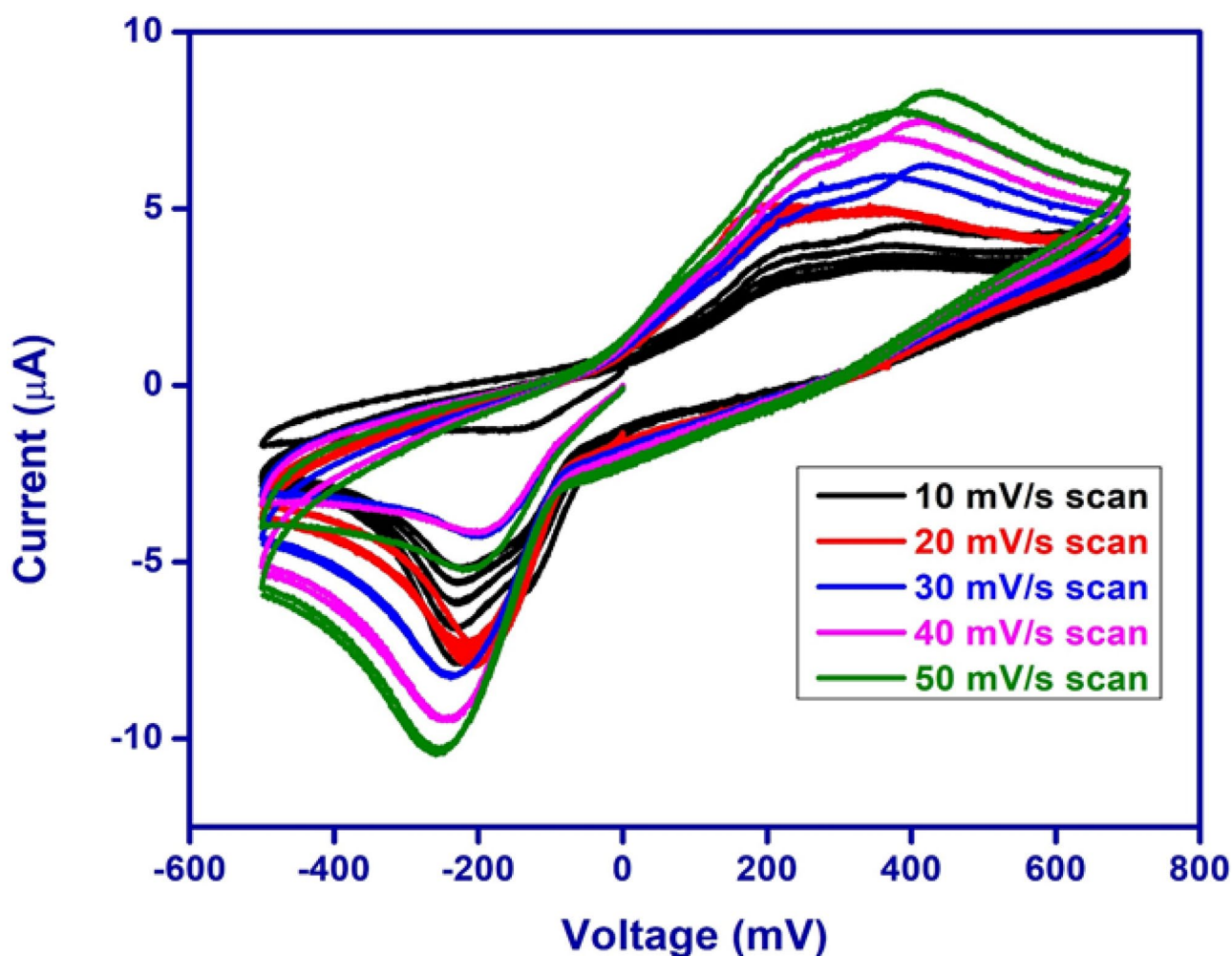
Fig. 6 Cyclic Voltammograms of PLZ4 with scan rates from 10 mV/s to 50 mV/s

The CV plots show a lot of stable current for voltage change and a lot of reversibility through reversing the polarity, which is great. Reversible humps in the CV curve can be seen at all scan rates, proving the capacitive behaviour and illuminating the redox reaction. These CV charts exhibit nearly constant current during the voltage ramp up and ramp down as well as the polarity flip, demonstrating the good reversibility of these n-LSPE membranes. The non-interactive behaviour of Li^+ ions with electrodes is confirmed by the disappearance of oxidation and reduction sharp peaks in CV-plots [14]. Furthermore, the peak currents in CV-plots increase significantly with an increase in scan rate. The shape distortion of the CV-plots was detected at high scan rates, and it was found to be caused by the currents becoming larger as the scan rate was raised, leading to the distorted shape. The capacitive behaviour decreases as the scan rate increases because the redox reaction occurs more quickly, limiting the migration of electrolyte ions into the active material. The data indicates that our n-LSPEs are an effective electrolyte for use in lithium ion batteries and capacitors [43–45]. Additionally, the

range of the PLZ4 sample's electrochemical stability window (ESW) was reported to be up to 1.2 V, which provides strong confirmation of the lack of faradic current effects.

Preparation of flexible electrochemical storage device (FESD)

Figure 7a depicts our FESD configuration with the $CuSO_4$ $5H_2O$ ‖ PVdF-HFP: PEO: $LiCF_3SO_3$: n-ZrO_2 ‖ V_2O_5 components. Copper and aluminium foils were used as anode and cathode current collectors, while the optimised lithium solid polymer electrolyte film PLZ4 served as a separator. Microwaveable PVC film is used for proper sealing, and solid polymer electrolyte membranes are sandwiched between cathode and anode materials. For the cathode, we used $CuSO_4$ $5H_2O$ (1000 mg) and PVdF-HFP polymer (100 mg) as binders. Cathode ingredients were mixed into THF solvent and heated to 40℃ while being stirred at a rate of 250 revolutions per minute for 12 h. The coated copper foil with gel serves as the cathode material. For the anode, we used
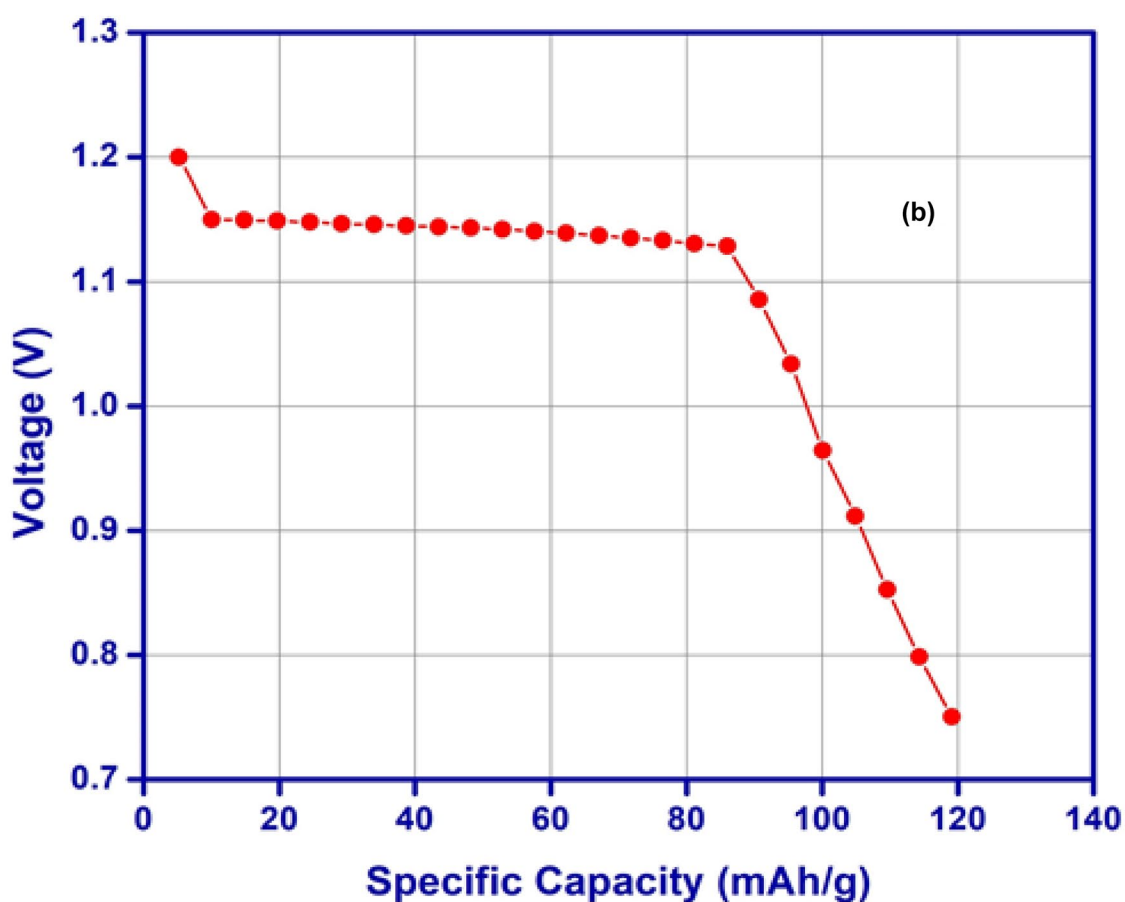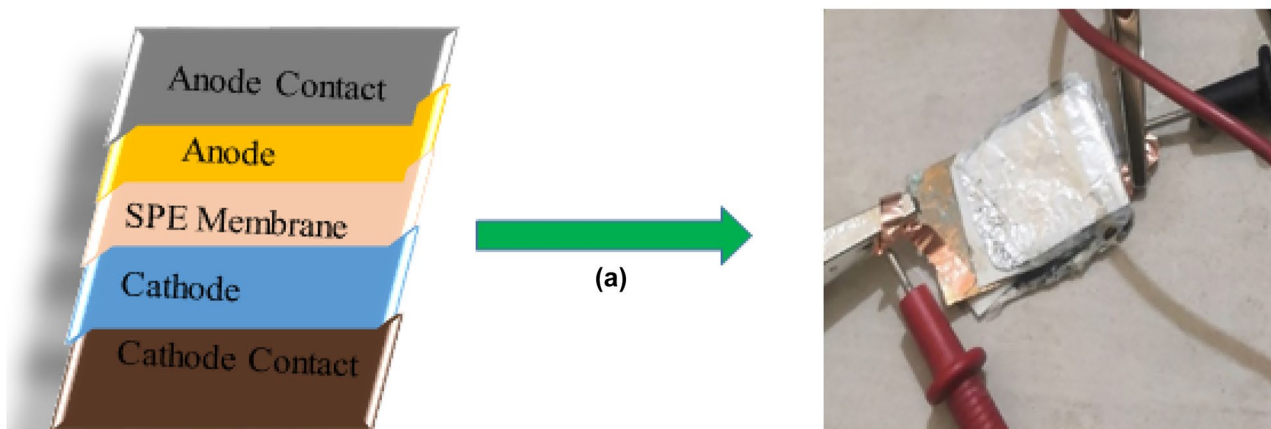
Fig. 7 **a** FESD device along with schematic interpretation **b** Discharge characteristics of FESD

V_2O_5 (1000 mg) and PVdF-HFP polymer (100 mg) as binders. For 12 h at 40℃ and a stirring rate of 250 rpm, the anode composition was dissolved in THF solvent. Anode material in the form of gel affixed to aluminium foil is ready for use. Figure 7b displays the results of FESD discharge characteristics. We were able to get an open circuit voltage (OCV) of

1.2 V by discharging it at its rated current of 0.04C for 25 hours, which amounted to an average current discharge of about 4.8 mA per hour. Our FESD demonstrated excellent voltage stability for up to 18 h, but after that, the electrochemical device's voltage dropped precipitously. Our FESD's current density and power density values have been

Table 3 FESD parameters

Parameters of FESD	Measured Values
Weight	1.90 g
Area	4 cm^2
Thickness	2.5 mm
Open Circuit Voltage	1.2 V
Average discharge current	4.8 mA
Current density	12 A/m^2
Power density	3.03 W/kg

determined. To summarise, Table 3. contains the estimated values and detailed descriptions of all FESD parameters [34].

Scanning electron microscopy

SEM images of ‖ PVdF-HFP: PEO: LiCF$_3$SO$_3$: n-ZrO$_2$ ‖ complexes with different ratios of n-ZrO$_2$ of were shown in Fig. 8 n-LSPEs surface morphology was substantially changed by increasing concentration of n-ZrO$_2$. The surface profile of polymer complexes becomes smoother with better segmental motion of polymeric chains adjustment for ion hopping due to addition of n-ZrO$_2$, and further it leads to increase the ion transport behaviour.

The porous network examination of prepared polymer complexes was accomplished by using Image-J software interpreting histogram analysis. All analysed histograms of PLZ1 to PLZ5 were shown in Fig. 9. Average pores size of PLZ membranes was calculated using following equation [50],

$$Perimeter \ of \ the \ pore = 2\,\Pi\,r \ = \Pi\,d \qquad (5)$$

whereas, r = radius of the pore, d = diameter of the pore.

$$Average \ pores \ diameter = \frac{Average \ pores \ Perimeter}{\pi} \qquad (6)$$

Analysing PLZ1 to PLZ5, the average pore diameter was determined to be 61.4 μm, 51.68 μm, 22.38 μm, 12.72 μm, and 18.23 μm, respectively. This reveals unequivocally that an optimised structure of PLZ4 protected a porous network with a high degree of connectivity with narrow size pores [51]. It is clearly evidences that as n-ZrO$_2$ concentration increases ion dissociation ability and smooth interconnecting porous network can be under hand by raise in amorphous nature and electrical properties of membranes. PLZ4 with high probability of interconnecting pores clearly evidences crosslinking of polymeric chains may smoothen ionic transport due to interaction of n-ZrO$_2$ with polymer complex [44, 50].

X-ray diffraction study

The X-ray crystallographs for the samples PLZ1, PLZ2, PLZ3, PLZ4, PLZ5 were detailed interaction of n-ZrO$_2$ concentration with ‖ PVdF-HFP: PEO: LiCF$_3$SO$_3$ ‖ complex using XRD studies and represented in Fig. 10. The characteristic peaks at 20.3° and 26.05° corresponds to (110) and (021) planes of α-phase of PVdF-HFP are well matched with α-phase of PVDF diffraction peaks [46]. The appeared diffraction peaks of n-ZrO$_2$ resembles stable strong monoclinic
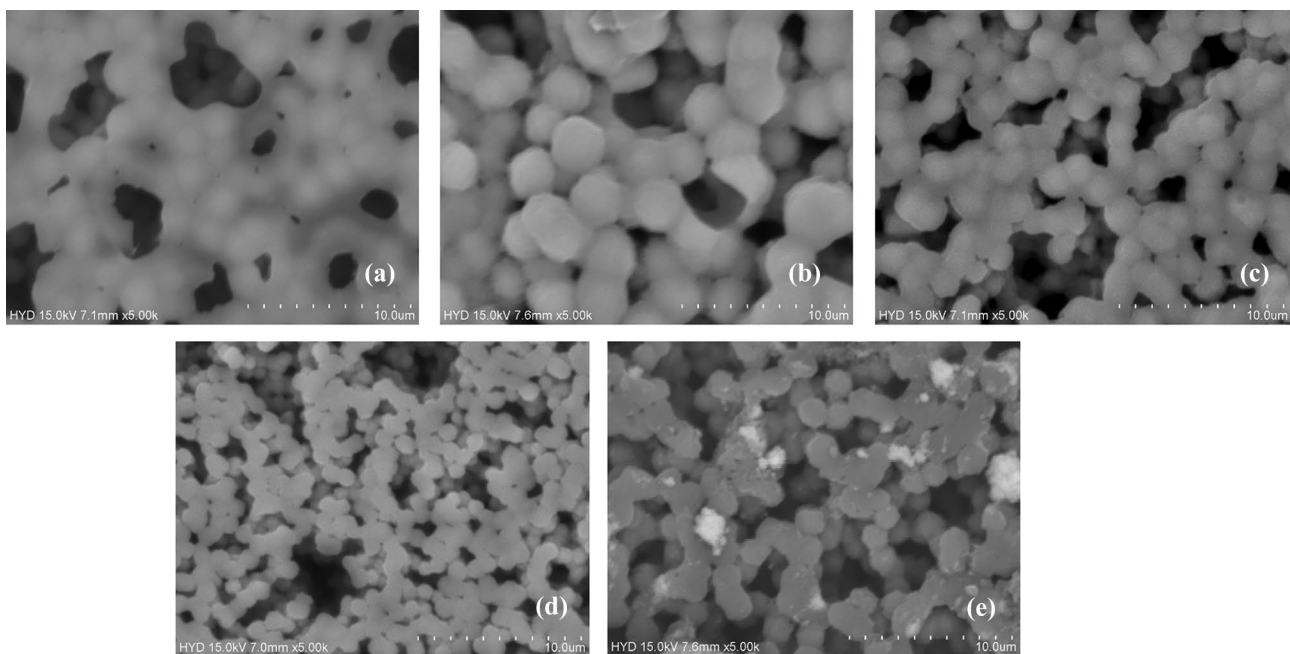

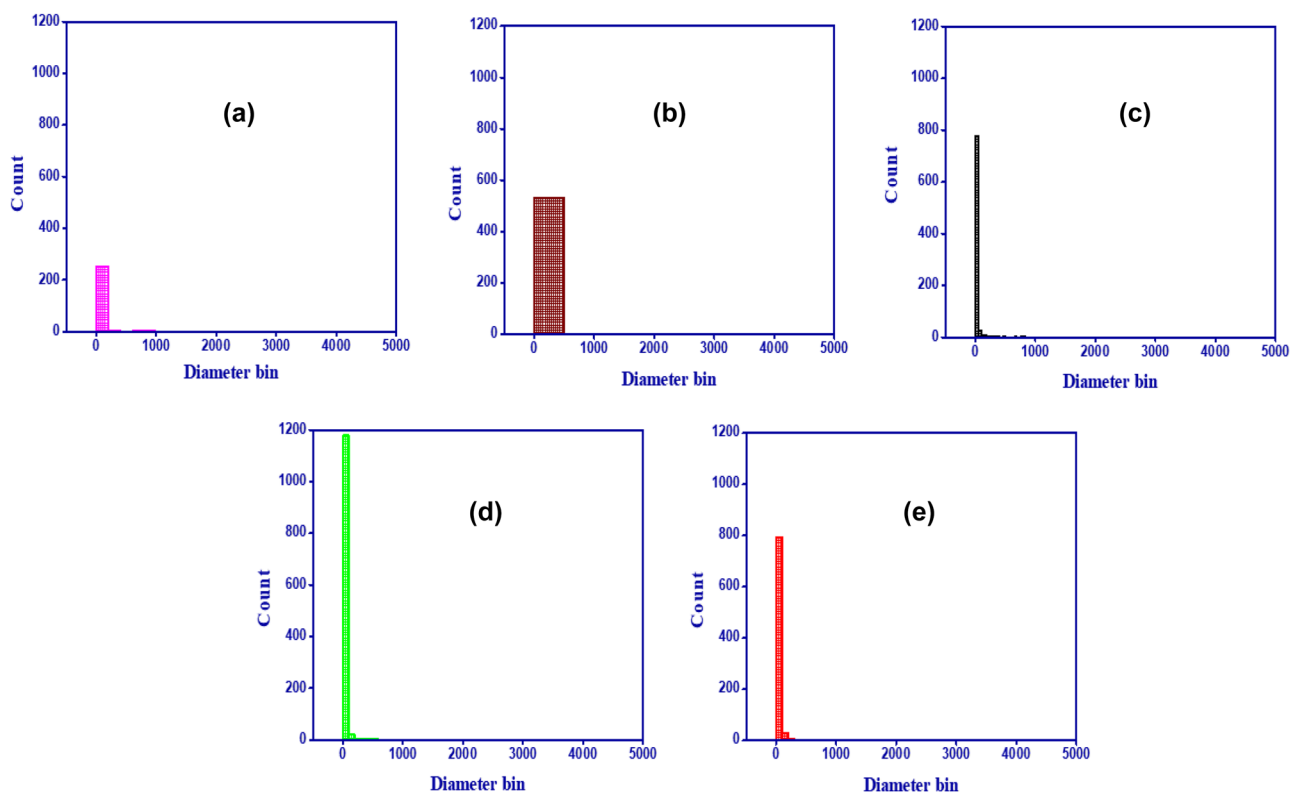**Fig. 8** SEM images with scan resolution of 10 μm of **a** PLZ1 **b** PLZ2 **c** PLZ3 **d** PLZ4 **e** PLZ5

Fig. 9 SEM histograms of **a** PLZ1 **b** PLZ2 **c** PLZ3 **d** PLZ4 **e** PLZ5

phase (m-ZrO$_2$) along with tetragonal phase (t-ZrO$_2$). The peaks at 28.47°, 31.7°, 54.4°, 55.6° owing to (-111), (111), (202), and (013) planes of m-ZrO$_2$. The corresponding peaks at 34.45°, 50.35°, 60.15° attributes (002), (202), and (311) planes of t-ZrO$_2$ [47]. It might prove that dominant polymeric segmental chain interactions are responsible for the disappearance or attenuation of n-ZrO$_2$ peaks.

Fourier transform infrared spectroscopy

The FTIR spectrographs of PLZ samples were recorded from 300 cm^{-1} to 2100 cm^{-1} shown in Fig. 11. The peak corresponds to 1641 cm^{-1} signifies stretching and bending vibration of H–O-H deformation mode from (-OH)$_n$ of polymer complex adsorbed on to ZrO$_2$ nano fillers. The vibrational frequencies 1267 cm^{-1}, 1182 cm^{-1}, 1035 cm^{-1} are owing to [υ_{as} (SO$_3$)], [υ_{as} (CF$_3$)], and [υ_s (SO$_3$)] of LiCF$_3$SO$_3$. The characteristic modes of n-ZrO$_2$ observed at 765 cm^{-1}, 646 cm^{-1}, 526 cm^{-1} due to Zr-O$_2$-Zr asymmetric stretching, Zr-O-Zr, Zr-O stretching modes confirms ZrO$_2$ phases [48, 49]. The modes attributed to [-OH], [υ_{as} (SO$_3$)], [υ_{as} (CF$_3$)], and Zr-O stretching were moved to lower wavenumber side, on the other hand Zr-O-Zr mode moved to higher wavenumber portion with increase of n-ZrO$_2$ concentration. The small

peak at 765 cm^{-1} due to Zr-O$_2$-Zr asymmetric stretching is stable (no shift) in all samples indicates monoclinic phase of n-ZrO$_2$ is corroborated with XRD. The mode corresponds [υ_s (SO$_3$)] with vibrational frequency of 1035 cm^{-1} strongly supports presence of high number of
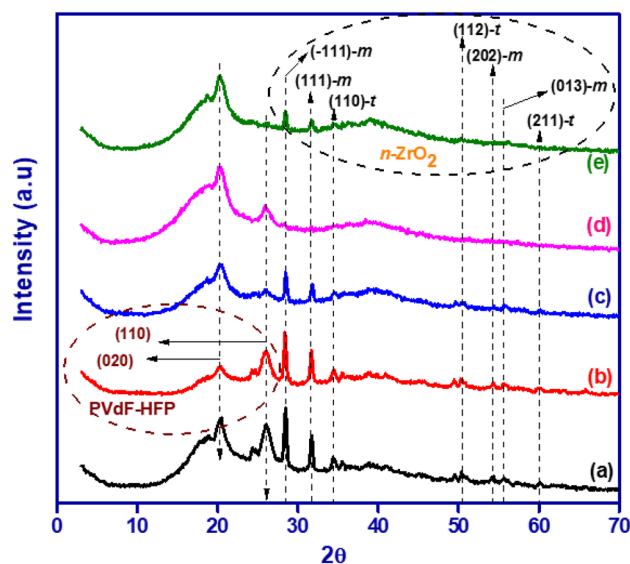

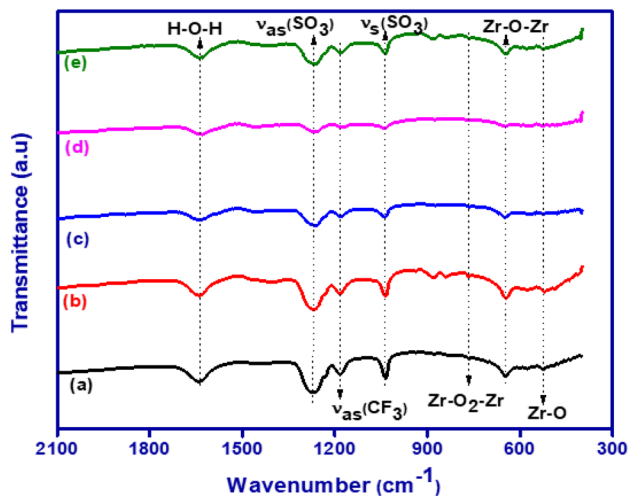**Fig. 10** XRD crystallographs of PLZ1, PLZ2, PLZ3, PLZ4, PLZ5

Fig. 11 **a** FTIR spectra of **a** PLZ1 **b** PLZ2 **c** PLZ3 **d** PLZ4 (f) PLZ5

mobile ions than ionic pairs. It is clear that the interaction of polymer complex functional groups with n-ZrO$_2$ results in highly compatible polymeric networks for ion transport via complexation in n-LSPEs. Further, we have estimated force constant, bond length values using following relations [50],

$$\upsilon = \frac{1}{2\pi c}\left(\frac{k}{\mu}\right)^{1/2} \tag{7}$$

υ-wave number, c- speed of light, k- force constant, μ -reduced mass respectively.

$$\text{Bond length(r)} = \sqrt[3]{\frac{17}{k}} \tag{8}$$

All the estimated values of bond lengths and force constants were tabulated in Table 4.

Table 4 Force constant and bond length values of functional groups present in n-LSPEs

FTIR mode	Wavenumber (cm^{-1})	Force constant (Mdynes/cm)	Bond length (A°)
HOH	1641	0.150675	4.824490421
υ_{as} (SO$_3$)	1267	1.011164	2.559375
υ_{as} (CF$_3$)	1182	0.606752	3.033869314
υ_s (SO$_3$)	1035	0.675803	2.92691
Zr-O$_2$-Zr	765	0.470112	3.302908439
Zr-O-Zr	646	0.33523	3.696580715
Zr-O	526	0.222254	4.238757243

Conclusions

The solution cast method was used to make n-LSPEs, which are lithium solid polymer blend electrolyte films doped with different weight ratios of n-ZrO$_2$. Using impedance measurements and dielectric spectroscopy, electrochemical analysis of prepared blend films reveals ionic transport behaviour. Electrochemical storage applications, such as batteries and capacitors, exhibit equivalent circuits in Cole–Cole plots, and our n-LSPEs have been shown to be highly suitable for these uses by means of impedance and dielectric spectroscopies. The electrochemical analysis results have all agreed that film PLZ4 is the best option for reaching the target conductivity of 5.996×10^{-1} mS/cm. The addition of n-ZrO$_2$ quadrupled the ionic conductivity of PLZ0. Inquiries into the ionic strength and voltage cyclic reversibility at different scan rates of PLZ4 using chronoamperometry and cyclic voltammetry confirmed its dominant ionic nature. The fact that PLZ4's ionic transference number is 0.963 shows that mobile Li$^+$ ions have a strong effect on ionic conductivity. Cross-linking, miscibility, and phase separation properties of n-ZrO$_2$ in polymer complexes were inferred from FTIR, XRD, and SEM analyses. Bond lengths and force constants of functional groups in fabricated n-LSPEs were calculated. The average size of the pores in PLZ4 is 12.72 μm, which exhibits a highly interconnected porous network between polymer chains corroborates high amorphous nature and better electrical properties. Discharge characteristics of fabricated flexible electrochemical storage device (FESD) were studied. The 0.04C rating signifies that our FESD's discharge characteristics were studied for 25 hours at an average discharge current of 4.8 mA. Nanocomposite lithium-based flexible electrochemical storage devices are intriguing to develop because they herald the dawn of a new era in smart electronics technology.

Declarations

Conflicts of interest There are no conflicts to declare.

References

1. Hu L, Wu H, Mantia FL, Yang Y, Cui Y (2010) ACS Nano 4:5843–5848. https://doi.org/10.1021/nn1018158
2. Yu X, Boyer MJ, Hwang GS, Manthiram A (2018) Chem 4:586–598. https://doi.org/10.1016/j.chempr.2017.12.029
3. Osiak M, Geaney H, Armstrong E, O'Dwyer C (2014) J Mater Chem A 2:9433. https://doi.org/10.1039/C4TA00534A

4. Pavithra MS, Prashanth JH, Taciana A, Bharat G, Prashant NK (2018) ACS Appl Energy Mater 1:483–494. https://doi.org/10.1021/acsaem.7b00094

5. Thomas S, Grohens Y, Jyotishkumar P (2015) Characterization of Polymer Blends: Miscibility, Morphology, and Interfaces, 1st edn. Wiley, New York

6. Sim LN, Majid SR, Arof AK (2012) Vib Spectrosc 58:57–66. https://doi.org/10.1016/j.vibspec.2011.11.005

7. Alipour M, Ziebert C, Conte FV, Kizilel R (2020) Batteries 6:35. https://doi.org/10.3390/batteries6030035

8. Negar Z, Khanmirzaei MH, Ramesh S, Ramesh K (2017) Mater Sci Semicond Process 66:144–148. https://doi.org/10.1016/j.mssp.2017.04.016

9. Mouraliraman D, Shaji N, Praveen S, Nanthagopal M, Ho CW, Karthik MV, Kim T, Lee CW (2022) Nanomaterials 12:1056. https://doi.org/10.3390/nano12071056

10. Yesappa L, Ashok kumar SP, Vijeth H, Basappa M, Sanjeev G, Devendrappa H (2019) J Radioanal Nucl Chem 322:05–10. https://doi.org/10.10907/s06466-0

11. Anil A, Sharma AL (2017) J Phys D: Appl Phys 50:443002. https://doi.org/10.1088/1361-6463/aa9f69

12. Reddy MR, Subrahmanyam AR, Reddy MM, Kumar JS, Kamalaker V, Reddy MJ (2016) Mater Today: Proc 3:3713–3718. https://doi.org/10.1016/j.matpr.2016.11.018

13. Danquah SA, Strimaitis J, Denize CF, Pradhan SK, Bahoura M (2022) Batteries 8:3. https://doi.org/10.3390/batteries8010003

14. Priyanka D, Sengwa RJ (2020) Ionics 26:1–17. https://doi.org/10.1007/s11581-019-03337-2

15. Jhuo HJ, Sunil S, Chen HL, Chen SA (2018) J Mater Chem A 6(19):8874–8879. https://doi.org/10.1039/C8TA01739E

16. Cheng YJ, Yang SH, Hsu CS (2009) Chem Rev 109(11):5868–5923. https://doi.org/10.1021/cr900182s

17. Wang HT, Xu P, Zhong W, Shen L, Du Q (2005) Polym Degrad Stabil 87:319–327. https://doi.org/10.1016/j.polymdegradstab.2004.08.015

18. Otsuka T, Chujo Y (2010) Polym Journal 42:58–65. https://doi.org/10.1038/pj.2009.309

19. Konakove VG et al (2016) Rev Adv Mater Sci 13:71

20. Garvie RC, Hannink RH, Pascoe RT (1975) Nature 258:703–704. https://doi.org/10.1038/258703a0

21. Hannink RH, Kelly PM, Muddle BC (2000) J Am Ceram Soc 83:461–487. https://doi.org/10.1111/j.1151-2916.2000.tb01221.x

22. Angham H, Ahmed H, Hayder A (2021) Nanosistemi Nanomateriali Nanotechnologii 18:983–1001

23 MusyarofahSoontaranon S, Limphirat W (2019) Triwikantoro, Pratapa S. Ceram Int 45:15660–15670. https://doi.org/10.1016/j.ceramint.2019.05.078

24. Mettu, MR, Mallikarjun A, Reddy MV, Reddy MJ, Kumar JS (2022) ICIMA, Springer Nature

25. Jeedi VR, Narsaiah EL, Yalla M, Swarnalatha R, Reddy SN, Chary AS (2020) SN Appl Sci 2:2093. https://doi.org/10.1007/s42452-020-03868-8

26. Kiran KG, Ramana JV, Kumar KV, Narsaiah EL (2021) Int J Polym Anal Charact 26:130–144. https://doi.org/10.1080/1023666X.2020.1860396

27. Sharma S, Pathak D, Dhiman N, Kumar R (2017) Surf Innov. https://doi.org/10.1680/jsuin.17.00019

28. Aziz SB, Brevik I, Hamsan MH, Brza MA, Nofal MM, Abdullah AM, Rostam S, Al-Zangana S, Muzakir SK, Kadir MFZ (2020) Polymers 12:2257. https://doi.org/10.3390/polym12102257

29. Brza MA, Shujahadeen BA, Anuar H, Ali F, Hamsan MH, Kadir MFZ, Rebar TA (2020) Arab J Chem 13:7247–7263. https://doi.org/10.1016/j.arabjc.2020.08.006

30. Ramesh S, Wen LC (2010) Ionics 16:255–262. https://doi.org/10.1007/s11581-009-0388-3

31. Alias AN, Kudin TIT, Zabidi ZM, Harun MK, Yahya MZA (2012) Adv Mater Res 501:39–43. https://doi.org/10.4028/www.scientific.net/AMR.501.39

32. Sengwa RJ, Priyanka D, Shobhna C (2014) Electrochim Acta 142:359–370. https://doi.org/10.1016/j.electacta.2014.07.120

33. Genova F, Subramanian S, Naranappa V, Sivadevi S, Manavalan P, Karthikeyan S (2017) Ionics 23:2727–2734. https://doi.org/10.1007/s11581-017-2052-7

34. Sampath KL, Christopher SP, Selvasekarapandian S (2021) Polym Bull 78:1797–1819. https://doi.org/10.1007/s00289-020-03185-5

35. Zhefei R, Yuzhe D, Hongfei P, Ruiming Z, Fangfang Z, Haolin T, Haining Z (2022) Polymers 14:1950. https://doi.org/10.3390/polym14101950

36. Margareta PG, Aleksovska S, Sandra DL, Marjan M (2016) Phys Scr 91:045805. https://doi.org/10.1088/0031-8949/91/4/045805

37. Govindaraj G, Baskaran N, Shahi K, Monoravi P (1995) Solid State Ion 76:47–55. https://doi.org/10.1016/0167-2738(94)00204-6

38. Singh KP, Gupta PN (1998) Eur Polym J 34:1023–1029. https://doi.org/10.1016/S0014-3057(97)00207-3

39. Padmasree KP, Kanchan DK, Kulkarni AR (2006) Solid State Ion 177:475–482. https://doi.org/10.1016/j.ssi.2005.12.019

40. Sinclair DC, West AR (1989) J Appl Phys 66:3850–3856. https://doi.org/10.1063/1.344049

41. Bard AJ, Faulkner LR (2000) Electrochemical methods: Fundamentals and Applications, 2nd edn. John Wiley & Sons

42. Dannoun EMA, Aziz SB, Brza MA, Al-Saeedi SI, Nofal MM, Mishra K, Abdullah RM, Karim WO, Hadi JM (2022) Int J Mol Sci 23:9152. https://doi.org/10.3390/ijms23169152

43. Yesappa L, Mydur N, Kumar SPA, Vijeth H, Basappa M, Jishnu D, Petwal V (2018) SGanesh S, Devendrappa H. RSC Adv 8:15297–15309. https://doi.org/10.1039/c8ra00970h

44. Teng S, Siegel G, Wang W, Tiwari A (2014) ECS Solid State Lett 3:M25. https://doi.org/10.1149/2.005405ssl

45. Alkhalaf S, Ranaweera CK, Kahol PK, Siam K, Adhikari H, Mishra SR, Perez F, Gupta BK, Ramasamy K, Gupta RK (2017) J Alloys Compd 692:59–66

46. Saikh Md, Hoque N, Biswas P, Rahman W, Das N, Das S, Thakur P (2021) Phys Status Solidi A 218:2000695. https://doi.org/10.1002/pssa.202000695.

47. Gonell F, David P, López BJ, Vallé K, Sanchez C, Corma A (2016) Catal Sci Technol 6:8257–8267. https://doi.org/10.1039/C6CY01082B

48. Wilson J, Ravi G, Kulandainathan A (2006) Polimeros 16:88–93. https://doi.org/10.1590/S0104-14282006000200006

49. Powers DA, Gray HB (1973) Inorg Chem 12:2721–2726. https://doi.org/10.1021/ic50129a045

50. Mallikarjun A, Kumar JS, Sreekanth T, Sangeetha M, Reddy MM, Sekhar EC, Reddy MJ (2022) J Polym-Plast Tech Mat 62:145–161. https://doi.org/10.1080/25740881.2022.2096471

51. Zhang H, Zhang G, Gao Q, Tang M, Ma Z, Qin J, Wang M, Kim JK (2020) Chem Eng J 379:122304. https://doi.org/10.1016/j.cej.2019.122304